Intramyocardial oxygen transport by quantitative diffuse reflectance spectroscopy in calves

Tobias Lindbergh
Marcus Larsson
Linköping University
Department of Biomedical Engineering
Division of Biomedical Instrumentation
Linköping, 58185 Sweden

Zoltán Szabó
Linköping University
Department of Medicine and Health Sciences
Division of Drug Research, Anesthesiology
Linköping, 58185 Sweden

Henrik Casimir-Ahn
Linköping University
Department of Medicine and Health Sciences
Division of Cardiovascular Medicine, Thoracic Surgery
Linköping, 58185 Sweden

Tomas Strömberg
Linköping University
Department of Biomedical Engineering
Division of Biomedical Instrumentation
Linköping, 58185 Sweden

Abstract. Intramyocardial oxygen transport was assessed during open-chest surgery in calves by diffuse reflectance spectroscopy using a small intramuscular fiber-optic probe. The sum of hemo- and myoglobin tissue fraction and oxygen saturation, the tissue fraction and oxidation of cytochrome aa3, and the tissue fraction of methemoglobin were estimated using a calibrated empirical light transport model. Increasing the oxygen content in the inhaled gas, 21%–50%–100%, in five calves (group A) gave an increasing oxygen saturation of 19±4%, 24±5%, and 28±8% ($p<0.001$, ANOVA repeated measures design) and mean tissue fractions of 1.6% (cytochrome aa3) and 1.1% (hemo- and myoglobin). Cardiac arrest in two calves gave an oxygen saturation lower than 5%. In two calves (group B), a left ventricular assistive device (LVAD pump) was implanted. Oxygen saturation in group B animals increased with LVAD pump speed ($p<0.001$, ANOVA) and with oxygen content in inhaled gas ($p<0.001$, ANOVA). The cytochrome aa3 oxidation level was above 96% in both group A and group B calves, including the two cases involving cardiac arrest. In conclusion, the estimated tissue fractions and oxygenation/oxidation levels of the myocardial chromophores during respiratory and hemodynamic provocations were in agreement with previously presented results, demonstrating the potential of the method.
[DOI: 10.1117/1.3374050]

Keywords: diffuse reflectance spectroscopy (DRS); oxygen transport; myocardium; hemoglobin; myoglobin; cytochrome c oxidase; cytochrome aa3; oxygenation; oxidation.

Paper 09179RR received May 7, 2009; revised manuscript received Feb. 8, 2010; accepted for publication Feb. 10, 2010; published online Apr. 19, 2010.

1 Introduction

A common reason for myocardial ischemia in heart patients is atherosclerotic coronary heart disease. Treatment often involves medication and/or surgical interventions, such as coronary stent implants and coronary artery bypass grafting (CABG). During the CABG procedure, the blood flow in the grafted vessels can be monitored during the surgery with ultrasound techniques.[1–3] However, for proper contractility in the myocardial cells, not only adequate coronary blood flow and release of hemoglobin-bound oxygen in capillaries, but also sufficient mitochondrial oxygen uptake has to be ensured.[4–6]

Optical steady-state diffuse reflectance spectroscopy (DRS) has been used in several *in vitro* studies to study myocardial tissue status via spectral changes that are linked to chromophores involved in myocardial oxygen transport.[7–10] A chromophore that reveals information about the mitochondrial oxygen uptake is the cytochrome aa3 (cyt aa3), also known as cytochrome c oxidase. This is an enzyme found in the mitochondrial inner wall and is the final electron transporter in the mitochondrial respiratory chain.[11] A reduction of the cyt aa3 oxidation status causes a decrease in cellular adenosine triphosphate (ATP) production. Therefore, monitoring of cyt aa3 oxidation status can be of vital importance in clinical cardiovascular medicine, since ATP production is a prerequisite for proper mechanical function in the myocardium.[12] Since the optical absorbances of reduced and oxidized cyt aa3 differ, DRS is suitable for detecting changes in cyt aa3 oxidation status. However, it is a nontrivial challenge to separate the absorption effects of cyt aa3 tissue fraction from that of hemoglobin,[13] although attempts have been made to measure the cyt aa3 oxidation status in the presence of hemoglobin.[14]

The redox state of nicotinamide adenine dinucleotide (NADH) has been described by Mayevsky and Chance as another marker in measuring mitochondrial function.[15] In that study, it was concluded that the best way of monitoring the NADH redox state is by fluorometry, and that when measurements are performed on biological systems, monitoring of the NADH redox state alone is not sufficient when determining the tissue vitality.

Until today, DRS techniques have relied on physiological provocations to establish reference situations involving com-

Address all correspondence to: Tobias Lindbergh, Linköping University, Department of Biomedical Engineering, Linköping, 58185 Sweden. Tel: 13-22-21-13; Fax: 13-1-19-02; E-mail: tobi@imt.liu.se.

1083-3668/2010/15(2)/027009/11/$25.00 © 2010 SPIE

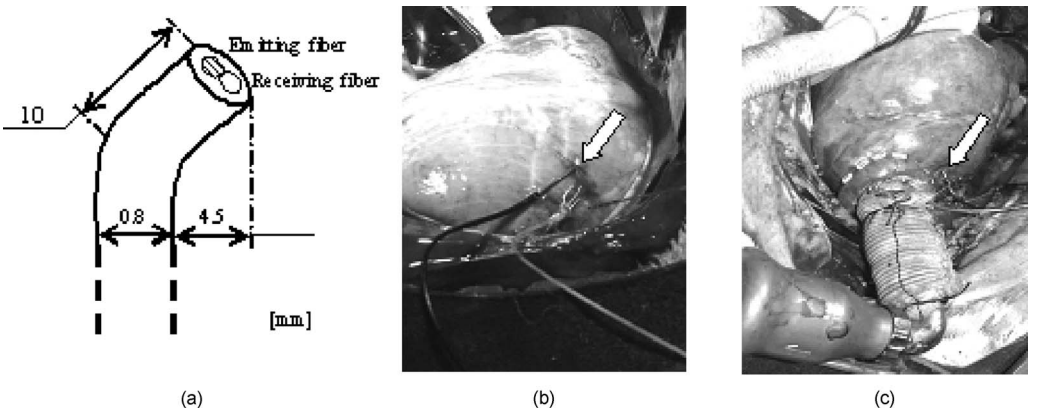

Fig. 1 (a) Probe design, indicating the dimensions of the probe tip. The hatched fiber indicates the emitting fiber. (b) Fiber-optic probe placement in animals from group A. (c) Fiber-optic probe placement in animals from group B, including the LVAD. The probe placement is highlighted with a white arrow.

plete oxidation and reduction of the cyt aa3,[16–18] while only relative changes in the oxidation status have been measured. Obviously, extreme physiological provocations for reference measurements are not possible in clinical patient monitoring. However, publication[19] of the specific extinction coefficients of cyt aa3 enables quantification of cyt aa3 tissue fraction and oxidation status without the need for physiological provocations.

The aim of this study was to determine the tissue fraction and oxygenation of the myocardial hemo- and myoglobin, the tissue fraction and oxidation of cytochrome aa3, and the tissue fraction of methemoglobin during hemodynamic and respiratory provocations in calves undergoing open-chest surgery. A small intramuscular fiber-optic probe and calibrated DRS was used for measurements during variations in the oxygen fraction of inhaled gas, when unloading the heart using a left ventricular assisting device (LVAD) and, in two calves, during cardiac arrest at the end of the experiment.

2 Material and Methods

Seven calves, 5 months old, body weight ranging from 75 to 85 kg, were used in this study. The animals were primarily enrolled in two different studies performed at the Animal Research Laboratory, Linköping University Hospital. Both studies were approved by the regional animal ethic committee.

The main purpose of the first study (group A) was to provide open-chest situations for ablation surgery training.

The main purpose of the second study (group B) was to implant and evaluate the performance of a left ventricle assisting device (LVAD) to be used in humans suffering from severe left ventricle heart failure.

In both studies, the calves were premedicated with xylazine hydrochloride (0.15 mg/kg) and atropine sulfate (0.06 mg/kg). A central venous catheter was inserted into the external jugular vein for administration of fluids and medication. Pentobarbital sodium (2 mg/kg) was used for induction of anesthesia, and a tracheotomy was carried out to allow mechanical ventilation. Anesthesia was maintained with intravenous fentanyl (10 μg/kg/h) and pentobarbital sodium (2 mg/kg/h).

2.1 *Surgical Technique*

Exposure of the heart was performed with a midline sternotomy. In group A, immediately after the sternotomy, the intramuscular fiber-optic probe was placed at a depth of approximately 5 mm in an area of the left ventricle wall supplied by the left anterior descending (LAD) artery. The probe was fixated by epicardial suturing in order to minimize movement artifacts.

In group B, extracorporeal circulation (ECC) was established after the sternotomy, and the aorta was cross-clamped together with antegrade cardioplegia infusion according to routine clinical procedures. The LVAD was implanted in the apex of the left ventricle. The aorta cross-clamp was then removed, and the LVAD was set to 6000 rpm. The intramuscular fiber-optic probe was then positioned identically as in animals in group A. For details about the implantation, see Hübbert et al.[20] A schematic drawing of the probe, including the dimensions, and the probe placement in both group A and group B animals are shown in Fig. 1.

2.2 *Equipment*

A multichannel spectrometer (AvaSpec 2048-5-RM, Avantes BV, Eerbeek, The Netherlands) operating in the visible wavelength region (400 to 900 nm, grating: VB 600 lines/mm), was used. Access to the tissue was gained through a custom-built fiber-optic probe containing one emitting and one receiving step-index multimode fiber with a core/cladding diameter of 200/230 μm and a numerical aperture of 0.37. The optical fibers were inserted into a slightly bent syringe cannula with a diameter of 800 μm (Fig. 1, left panel). The receiving fiber was positioned adjacent to the illuminating fiber at a center–center separation of 230 μm. An additional fiber, guiding light directly from the lamp to the spectrometer, was used for registering the spectrum of the light source. In-house designed algorithms and software were developed for data recording and analysis, using LabView 6.1 (National Instruments, Austin, Texas), and MATLAB 7.5 (Mathworks, Inc., Natick, Massachusetts), respectively.

2.3 *Protocols and Spectral Recordings*

For each measured spectrum, a simultaneous registration of the lamp spectrum was performed. The integration time was not changed during each case, but varied from 200 ms to 1000 ms between calves.

After finishing the measurements on each subject, before disconnecting the probe from the spectroscope, three reference measurements were performed. As reference, a tightly packed sample of barium sulfate ($BaSO_4$) powder with a reflectivity of above 98% in the visible wavelength range was used. The probe was vertically lowered approximately 1 cm into the powder, allowing no surrounding light to enter. Three consecutive 10-s measurements were performed. Last, the lamp was turned off, and a dark spectrum (D) was registered.

2.3.1 *Group A (provocations with changes in $F_{I,O2}$)*

Five calves, denoted A1 to A5, were subjected to this protocol. After placement of the fiber-optic probe, at least 10 min was allowed to achieve stable heart rhythm as assessed by visual inspection of the ECG signal. In calves A1 and A2, the surgical training protocol was carried out before the spectroscopic measurements in order to enable measurements during cardiac arrest in the end of the experiment. In calves A3 to A5, measurements were performed immediately after the 10-min stabilization phase and before the surgical training.

The fraction of inspired O_2 ($F_{I,O2}$) was varied in three different steps, 21%, 50%, and 100%, respectively, with 3-min duration per phase. Spectra were measured continuously during the $F_{I,O2}$ variations. In cases A1 and A2, registrations of spectra during 3 to 4 min after initiation of cardiac arrest in the end of the experiment were also performed.

2.3.2 *Group B (provocations with changes in LVAD speed and $F_{I,O2}$)*

Two calves, denoted B1 and B2, were subjected to this protocol. Similar to the group A protocol, at least 10 min of stable heart rhythm was allowed after placement of the fiber-optic probe.

In calve B1, the $F_{I,O2}$ was first held constant at 100%, while the speed of the LVAD was varied in three different steps, 6000 rpm, 7500 rpm, and 10,000 rpm, with 1-min duration per phase. After switching from 6000 rpm to 7500 rpm, and from 7500 rpm to 10,000 rpm, 30 s was allowed before spectra were measured.

After the 1-min duration with the LVAD speed at 10,000 rpm, the $F_{I,O2}$ was then varied in four steps; 50%, 21%, 50%, and 100%, with 1-min duration per phase. During the different $F_{I,O2}$ levels, spectra were measured continuously.

In calf B2, the LVAD speed was held constant at 7500 rpm throughout the experiment, and $F_{I,O2}$ was varied in three different steps, 21%, 50%, and 100%, with 1-min duration per phase.

2.4 *Spectral Preprocessing and System Calibration*

First, all unprocessed measurement spectra M^{raw} were dark-corrected by subtracting the detector dark noise spectrum, D, which was registered immediately after each measurement series. The dark-corrected spectra ($M^{raw}-D$) were then filtered and resampled in three preprocessing steps: first, the spectrum was equidistantly up-sampled to a resolution of 0.1 nm; second, high-frequency noise and aliasing effects were removed using a phase-invariant low-pass filter (Butterworth of order 4) with a normalized cutoff frequency of 0.02; and third, the spectra was down-sampled to a resolution of 1 nm and limited to the wavelength region 500 to 800 nm. Visual inspection of the residuals when comparing unfiltered and filtered data displayed only stochastic noise with no trends or patterns. To eliminate influences from changes in lamp intensity and color, all preprocessed measurement spectra were normalized by simultaneously recorded and preprocessed lamp spectra. The unprocessed white reference measurements (M^{raw}_{white}) were identically preprocessed and normalized, and in addition, averaged over time in order to obtain a single white reference spectrum. Last, the lamp-normalized measurement spectra were white-corrected by dividing with the lamp-normalized time-averaged white spectra. The complete normalization process is described in Eq. (1):

$$M^{norm}_{heart} = \frac{(M^{raw}_{heart} - D_{heart}/M^{raw}_{lamp,heart} - D_{heart})}{\langle M^{raw}_{white} - D_{white}/M^{raw}_{lamp,white} - D_{white}\rangle_t}, \quad (1)$$

where $\langle\cdot\rangle_t$ denotes averaging over time. The preprocessed and normalized spectrum M^{norm}_{heart} was used in the analysis of myocardial tissue status.

The method used for calibration was originally described by Jacques[21] and has, with some modifications, been used by other authors.[22,23] The details are described in Häggblad et al.,[22] and only a brief overview is given here. The method utilizes a modified Beer-Lambert model that takes both absorption and scattering into account when describing the light transport, T, in tissue. The expression is given in Eq. (2):

$$T(\mu_a, \mu_s') = K \cdot \exp(-\mu_a \cdot L), \quad (2)$$

where $K=a+b\cdot\mu_s'+c\cdot\mu_s'^2$, and $L=d+e\cdot\mu_s'+f\cdot\mu_s'^2$, with a to f being constants determined in a calibration procedure involving measurements on liquid optical phantoms based on milk (scatterer), ink (absorber), and distilled water. The optical properties of the phantom grid were $\mu_s=[1\ 2\ 3\ 4\ 8]_{\lambda=632.8\ nm}\ mm^{-1}$, $\mu_a=[0\ 0.01\ 0.05\ 0.1\ 0.2\ 0.4\ 0.8\ 1.6]_{\lambda=632.8\ nm}\ mm^{-1}$. The anisotropy factor, g, of milk at 632.8 nm was set to 0.84 according to a previous study,[24] resulting in $\mu_s'=[0.16\ 0.32\ 0.64\ 1.28]_{\lambda=632.8\ nm}\ mm^{-1}$. The calibrated light transport model was denoted T_{cal}.

2.5 *Tissue Chromophore Selection and Spectral Analysis*

The major chromophores in myocardial tissue are oxygenized and deoxygenized hemoglobin and myoglobin (HbO_2, Hb, MbO_2, and Mb, respectively), water (W), and fat (lipid).[7,14,22] In addition to the major chromophores described earlier, it has been shown that methemoglobin (metHb) and changes in oxidation status of cyt aa3 in the myocardium can be detected by DRS.[10,18,25] To investigate whether inclusion of these additional chromophores resulted in a substantially improved model, two different setups were evaluated: one with only the major chromophores (Hb, HbO_2, Mb, MbO_2, and W) included in the absorption model (model I); and one including,

in addition to the major chromophores, metHb and the oxidized (cyt aa3,ox) and reduced (cyt aa3,red) form of cyt aa3 (model II). In this study, lipid absorption was not included in the light transport model because of its very low intramuscular concentration[26,27] compared to the epicardial fat layer.[22] According to several studies, the water content was set to 75% (Refs. 21, 22, and 28). Because of the very similar absorption spectra of hemoglobin and myoglobin (Mb is redshifted 2 to 4 nm compared to Hb), only the sum of the tissue fractions of these two chromophores was determined. However, to account for this shift, hemoglobin absorption spectra, with an adaptive wavelength transition of ±5 nm, was used in our absorption model [Eq. (3)]. The adaptive transition was implemented as a fitting parameter when solving the inverse problem. Equation (3) shows the expression for the total myocardial tissue absorption ($\mu_{a,\mathrm{heart}}$) for model II. The μ_a expression for model I is obtained by forcing $f_{\mathrm{cyt\ aa3}}$ and f_{metHb} to be equal to zero.

$$\begin{aligned}\mu_{a,\mathrm{heart}}(\lambda) = {} & f_{\mathrm{Hb+Mb}} \cdot [S_{\mathrm{Hb+Mb}} \cdot \mu_{a,\mathrm{HbO_2}} + (1 - S_{\mathrm{Hb+Mb}}) \cdot \mu_{a,\mathrm{Hb}}] \\ & + f_{\mathrm{cyt\ aa3}} \cdot [O_{\mathrm{cyt\ aa3}} \cdot \mu_{a,\mathrm{cyt\ aa3,ox}} \\ & + (1 - O_{\mathrm{cyt\ aa3}}) \cdot \mu_{a,\mathrm{cyt\ aa3,red}}] + f_{\mathrm{metHb}} \cdot \mu_{a,\mathrm{metHb}} \\ & + 0.75 \cdot \mu_{a,W}. \end{aligned} \quad (3)$$

In Eq. (3), $f_{\mathrm{Hb+Mb}}$ is the Hb+Mb tissue fraction, $S_{\mathrm{Hb+Mb}}$ is the Hb+Mb oxygen saturation, $f_{\mathrm{cyt\ aa3}}$ is the cyt aa3 tissue fraction, $O_{\mathrm{cyt\ aa3}}$ is the oxidation status of cyt aa3, and f_{metHb} is the metHb tissue fraction. It should be noted that absorption data is often provided in terms of the specific extinction coefficient, μ_e. The conversion from μ_e to μ_a can be found in Sec. 6.

The reduced scattering coefficient (μ_s') was modeled according to a previous study by Häggblad[22]:

$$\mu_s'(\lambda) = \frac{\alpha \cdot \lambda^{-\beta}}{700^{-\beta}}, \quad (4)$$

where α and β are the fitting parameters.

By combining T_{cal} and Eq. (3), expressions for light transport in myocardial tissue are obtained for both models and are denoted $T_{\mathrm{cal,I}}$ and $T_{\mathrm{cal,II}}$, respectively. The unknown parameters in Eqs. (3) and (4) ($f_{\mathrm{Hb+Mb}}$, $S_{\mathrm{Hb+Mb}}$, $f_{\mathrm{cyt\ aa3}}$, $O_{\mathrm{cyt\ aa3}}$, f_{metHb}, α, and β) were determined by minimizing the expressions $T_{\mathrm{cal,I}}/M_{\mathrm{heart}}^{\mathrm{norm}} - 1$ and $T_{\mathrm{cal,II}}/M_{\mathrm{heart}}^{\mathrm{norm}} - 1$ in a least-squares sense using the Levenberg-Marquardt algorithm. The Levenberg-Marquardt algorithm has been shown useful when solving nonlinear systems in a least-squares sense.[29]

The model spectra giving the optimum solutions were denoted $T_{\mathrm{cal,I}}^*$ and $T_{\mathrm{cal,II}}^*$, respectively. For both models, visual inspection of $T_{\mathrm{cal}}^*/M_{\mathrm{heart}}^{\mathrm{norm}} - 1$ was performed, and the goodness of fit was evaluated by calculating the Pearson product-moment correlation coefficient R^2. Visual inspection of $T_{\mathrm{cal}}^*/M_{\mathrm{heart}}^{\mathrm{norm}} - 1$ is a very intuitive way of identifying wavelength interval where the model fails to fit the measured data. In turn, this reveals information about possible missing chromophores in the light transport model.

The absorption data of hemoglobin and water were compiled from Zijlstra et al. and Buiteveld et al.,[30,31] respectively. The absorption data for cyt aa3,ox and cyt aa3,red were compiled from the BORL home page,[19] and absorption data for metHb was compiled from Zijlstra et al.[30] As the cyt aa3 absorption data were not available for wavelengths shorter than 520 nm (Ref. 19), while the sensitivity of the spectrometer was considered too poor above 800 nm, the spectral analysis was limited to the wavelength region 520 to 800 nm.

In group A, spectra from the last minute of each $F_{\mathrm{I,O2}}$ level were averaged over time, and the curve-fitting was applied on the resulting spectra. In group B, spectra from the last 10 s of each $F_{\mathrm{I,O2}}$ level and LVAD speed were averaged over time, and the curve-fitting was applied on the resulting spectra.

2.6 *Statistical Analysis*

Summarized data from groups A and B are calculated from fitting an average spectrum over the recording interval. The effect of $F_{\mathrm{I,O2}}$ on $S_{\mathrm{Hb+Mb}}$ (groups A and B) was evaluated on data from fitting individual spectra using an ANOVA repeated measures design, with calves and $F_{\mathrm{I,O2}}$ as factors. The effect of LVAD pump speed on $S_{\mathrm{Hb+Mb}}$ (calf B1) was evaluated on data from fitting individual spectra using an ANOVA repeated measures design, with subject and LVAD pump speed as factors.

3 Results

3.1 *Spectral Fitting*

To illustrate the effect of adding cyt aa3 and metHb as chromophores in the light transport model, two spectra with varying $S_{\mathrm{Hb+Mb}}$ were selected. The curve-fits for model I (dashed black), model II (solid black), and the measured spectrum (solid gray) are shown in Figs. 2 and 3.

Model I yielded characteristic spectral misfits in the wavelength region ~540 to ~620 nm. The use of model II resulted in improved spectral fitting, and the characteristic spectral misfits were eliminated. The calculated $S_{\mathrm{Hb+Mb}}$ using model II, compared to $S_{\mathrm{Hb+Mb}}$ from model I, differed only by –0.9% in the low $S_{\mathrm{Hb+Mb}}$ case (16.7% compared to 17.6%, respectively), and by 2.6% in the high $S_{\mathrm{Hb+Mb}}$ case (37.7% compared to 35.1%, respectively). The corresponding values for differences in $S_{\mathrm{Hb+Mb}}$ were 0.1% in both the high and low $f_{\mathrm{Hb+Mb}}$ case. The R^2-values for the two different curve-fits versus measured spectra from the last minute of phase $F_{\mathrm{I,O2}}$=21% of group A calves showed that model II resulted in higher R^2-values in all five cases ($R^2 > 0.99$). Taken together, the improved R^2-values and the eliminated spectral misfit characteristics in the residuals supported the choice of model II for further analysis. The wavelength shift in the Hb spectrum was on average in group A 2.2 nm, 2.0 nm, and 1.8 nm during $F_{\mathrm{I,O2}}$=21%, 50%, and 100%, respectively. In group B, the average wavelength shift was 0.8 nm.

3.2 *Intramyocardial Light Scattering*

The parameters α and β in Eq. (4) were averaged for each calf. In group A, μ_s' ranged from 0.17 $\mathrm{mm^{-1}}$ to 2.28 $\mathrm{mm^{-1}}$, and β was in the range 2.43 to 2.84. Corresponding values for group B were 0.35 $\mathrm{mm^{-1}}$ to 2.28 $\mathrm{mm^{-1}}$ (μ_s') and 2.18 to 3.91 (β). The average μ_s' calculated for both groups was 0.79 $\mathrm{mm^{-1}}$ at 633 nm and 0.45 $\mathrm{mm^{-1}}$ at 780 nm, which are both commonly used laser wavelengths in biomedical optics.

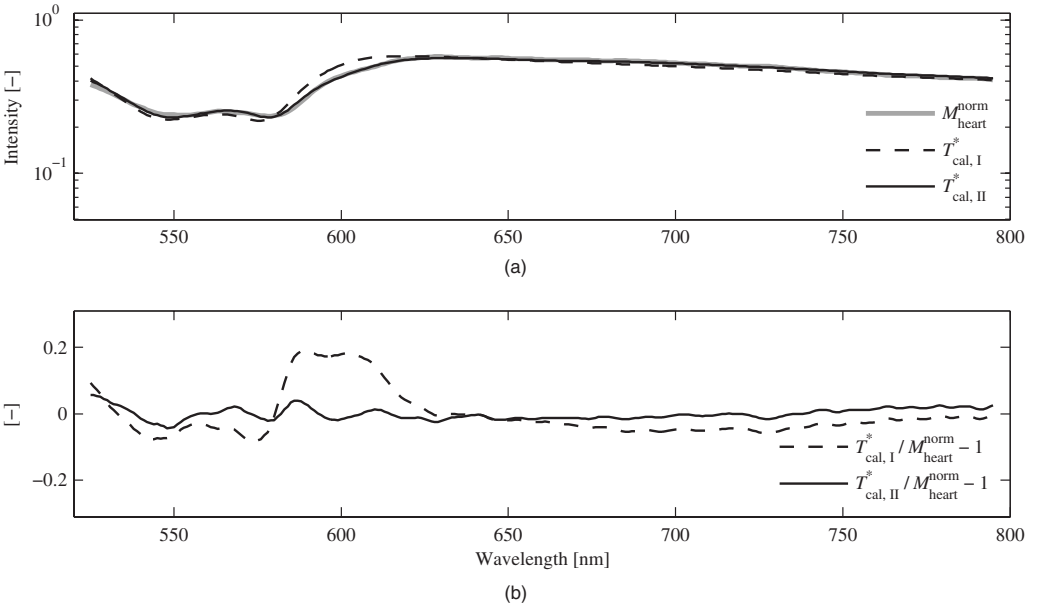

Fig. 2 (a) Representative measured spectrum (M^{norm}_{heart}) and model spectra ($T^{*}_{cal,I}$ and $T^{*}_{cal,II}$) from calf A4, 100% $F_{I,O2}$. (b) $T^{*}_{cal}/M^{norm}_{heart}-1$.

3.3 *Intramyocardial Tissue Chromophores*

The results for chromophore tissue fractions and oxygenation/oxidation status are presented for each group (A and B) separately. In addition, for group B, results for the two calves are presented as separate cases.

3.3.1 *Group A (provocations with changes in $F_{I,O2}$)*

As a representative case, Fig. 4 shows the time-resolved S_{Hb+Mb} for calf A2 during the variations in $F_{I,O2}$.

As can be seen in Fig. 4, there is an increase in S_{Hb+Mb} that follows the $F_{I,O2}$ changes from 21% via 50% to 100%. Approximately 60 s after each change, the S_{Hb+Mb} reached a stable value, suggesting that the S_{Hb+Mb} during the last 60 s of each $F_{I,O2}$ level is an accurate interval when calculating average S_{Hb+Mb} values for each $F_{I,O2}$.

Cyclic variations in S_{Hb+Mb} and f_{Hb+Mb} were detected throughout the measurements for all cases, although with varying magnitude of the variation. As an illustrative example of a case with high variation, f_{Hb+Mb} for the first 30 s of calf A1, is shown in the left panel of Fig. 5. The right panel illustrates the correlation between f_{Hb+Mb} and S_{Hb+Mb} during the same period.

The left panel in Fig. 5 shows distinct periodical behavior of f_{Hb+Mb}. The number of local maxima was determined by

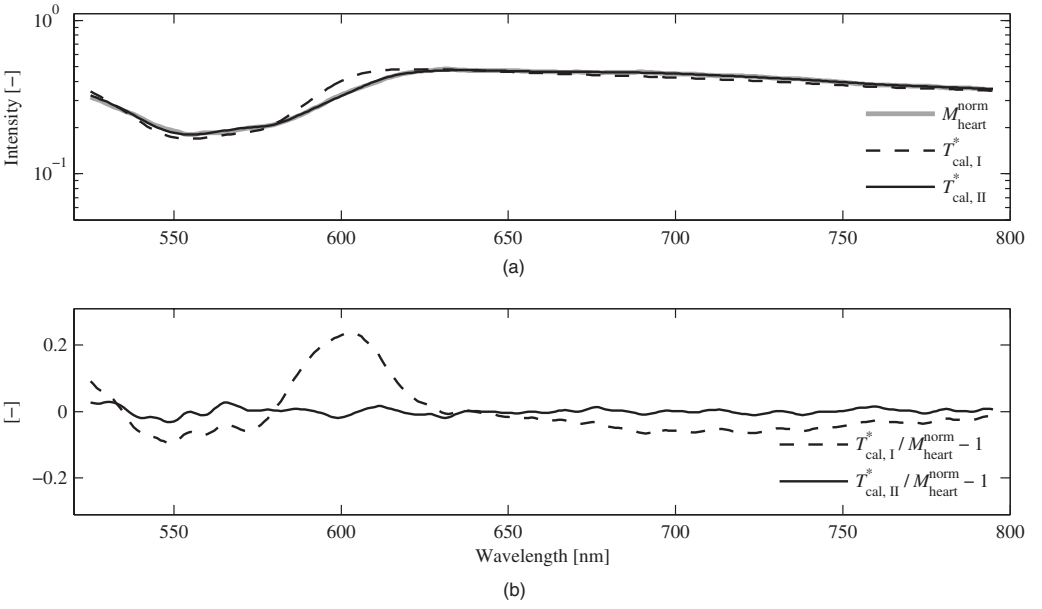

Fig. 3 (a) Representative measured spectrum (M^{norm}_{heart}) and model spectra ($T^{*}_{cal,I}$ and $T^{*}_{cal,II}$) from calf A4, 21% $F_{I,O2}$ (gray). (b) $T^{*}_{cal}/M^{norm}_{heart}-1$.

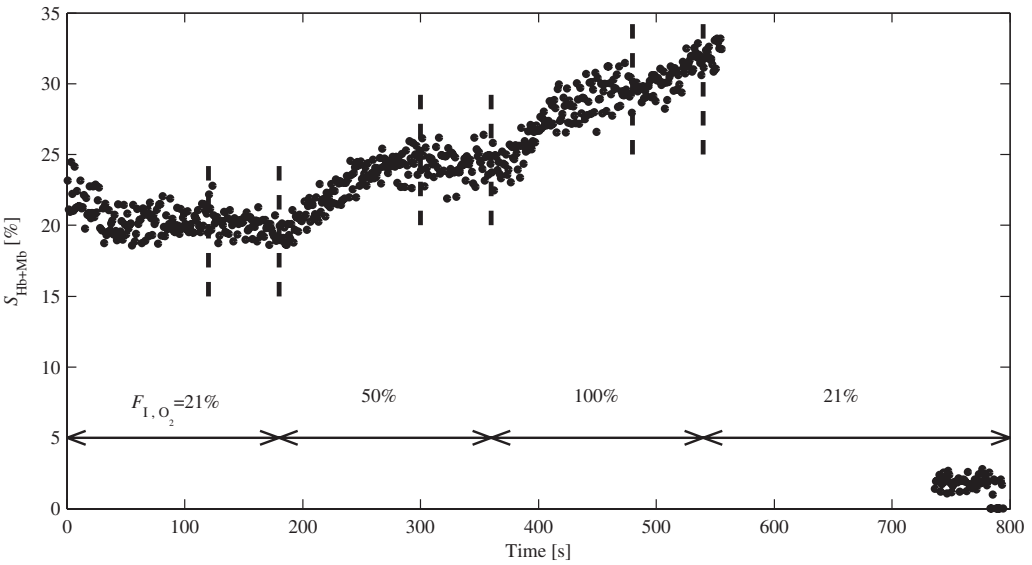

Fig. 4 S_{Hb+Mb} in calf A2 as a function of time during three different $F_{I,O2}$ and during cardiac arrest at the end of the experiment. The last minute in each $F_{I,O2}$ phase is marked with vertical dashed lines.

visual inspection to 34 during 30 s, giving a frequency of 68 min^{-1}. This was compared to the heart rate observed by the ECG monitor, which was 67 beats$\cdot min^{-1}$. The right panel displays an inverse relationship between f_{Hb+Mb} and S_{Hb+Mb}. The R^2-value of the fitted straight line was 0.94. Negative correlations between f_{Hb+Mb} and S_{Hb+Mb} were found for four of five calves. Similarly, the relationship between the wavelength shift of the Hb spectrum and the S_{Hb+Mb} was evaluated in order to determine whether the wavelength shift could be related to Mb during blood volume pulsations. However, the correlation between the wavelength shift and S_{Hb+Mb} was slightly positive in calves A1 to A3, slightly negative in A4, and without any trend in A5.

f_{Hb+Mb}, S_{Hb+Mb}, f_{metHb}, and $f_{cyt\ aa3}$ average values (over the last minute) of each $F_{I,O2}$ level are presented in Table 1. $O_{cyt\ aa3}$ was on average 97%, ranging from 82% to 100%, and displayed no correlations with $F_{I,O2}$. Thus, $O_{cyt\ aa3}$ data were omitted from Table 1.

As can be seen in Table 1, calves A1 to A4 responded with an increase in S_{Hb+Mb} when $F_{I,O2}$ increased. Increasing $F_{I,O2}$ 21% to 50% to 100%, gave average values for S_{Hb+Mb} $=19\pm4\%$, $24\pm5\%$, and $28\pm8\%$, respectively. Hence, the average increases in S_{Hb+Mb} were 4.6% and 4.5% when $F_{I,O2}$ was increased from 21% to 50% and from 50% to 100%, respectively. The effect of $F_{I,O2}$ on S_{Hb+Mb} was significant

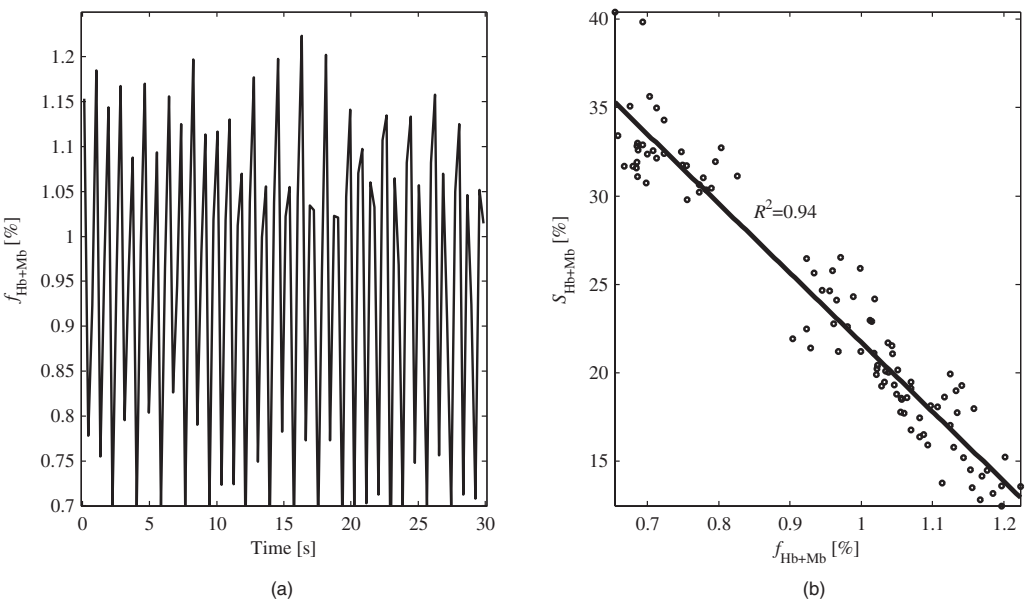

Fig. 5 (a) f_{Hb+Mb} as a function of time during the first 30 s in calf A1. (b) Relationship between f_{Hb+Mb} and S_{Hb+Mb} including linear fitting (R^2=0.94) during the first 30 s in calf A1.

Table 1 Average chromophore tissue fractions and S_{Hb+Mb} for the last minute of every $F_{I,O2}$ level.

		Calves					
$F_{I,O2}$ [%]	[%]	A1	A2	A3	A4	A5	Average
21	f_{Hb+Mb}	0.9	1.2	0.5	1.2	1.5	1.1
	S_{Hb+Mb}	22.8	20.0	22.6	14.7	15.6	19.1
	f_{metHb}	0[c]	0.1	0[c]	0[c]	0[c]	0[c]
	$f_{cyt\ aa3}$	1.5	1.7	1.3	1.9	2.0	1.7
50	f_{Hb+Mb}	0.9	1.3	0.5	1.2	1.6	1.1
	S_{Hb+Mb}	27.9	24.4	27.7	16.7	21.6	23.7
	f_{metHb}	0[c]	0.1	0[c]	0[c]	0[c]	0[c]
	$f_{cyt\ aa3}$	1.6	1.8	1.2	1.7	1.8	1.6
100	f_{Hb+Mb}	0.9	1.2	0.5	1.1	1.5	1.0
	S_{Hb+Mb}	33.3	30.4	32.5	31.1	13.8	28.2
	f_{metHb}	0.1	0.1	0[c]	0[c]	0[c]	0[c]
	$f_{cyt\ aa3}$	1.4	1.9	1.2	1.4	2.0	1.6
21[a]	f_{Hb+Mb}	1.4	1.1	—	—	—	—[b]
	S_{Hb+Mb}	3.7	1.8	—	—	—	—[b]
	f_{metHb}	0[c]	0.1				—[b]
	$f_{cyt\ aa3}$	1.4	2.0	—	—	—	—[b]

[a]For calves A1 and A2, $F_{I,O2}$ was set to 21% during the process of cardiac arrest in the end of the experiment. The average S_{Hb+Mb} was calculated during the time interval 3 to 4 min after initiation of cardiac arrest.
[b]No average values were calculated—only two values.
[c]Calculated values were smaller than 0.05%.

($p<0.001$, ANOVA). The S_{Hb+Mb} varied between calves ($p<0.001$, ANOVA), as did the response to $F_{I,O2}$ ($p<0.001$, ANOVA). Calves A1 to A3 had a similar stepwise increase in their S_{Hb+Mb}, while for A4, a larger response was seen when $F_{I,O2}$ increased from 50% to 100% than from 21% to 50%. For A5, S_{Hb+Mb} decreased when $F_{I,O2}$ increased from 50% to 100%.

3.3.2 *Group B (provocations with changes in LVAD speed and $F_{I,O2}$)*

The time-resolved S_{Hb+Mb} for calf B1 is shown in Fig. 6. It can be seen in Fig. 6 that the S_{Hb+Mb} did not reach stable levels during the O_2 provocations (180 to 480 s). For this reason, spectra from the 10 last seconds for every $F_{I,O2}$ level were averaged when calculating the tissue fractions and S_{Hb+Mb} and $O_{cyt\ aa3}$ levels of the chromophores. $O_{cyt\ aa3}$ was on average 98%, ranging from 84% to 100% throughout measurements in calf B1, and displayed no correlations with $F_{I,O2}$. The time-resolved S_{Hb+Mb} for calf B2 is shown in Fig. 7.

A similar oxygenation trend as in group A was observed during the O_2 variations. It should be noted that during the first $F_{I,O2}$ level (21%; 0 to 60 s), S_{Hb+Mb} did not reach a stable level. As in calf B1, spectra from the last 10 s were averaged when calculating chromophore tissue fractions and S_{Hb+Mb} and $O_{cyt\ aa3}$ levels. The chromophore tissue fractions and S_{Hb+Mb} oxygenation levels for both calves are summarized in Table 2. $O_{cyt\ aa3}$ was on average 96%, ranging from 85% to 100%, throughout the measurements in calf B2, and are omitted in Table 2.

In calf B1, only a small increase from 18.8% to 20.7% was found in S_{Hb+Mb} when increasing the LVAD speed from 6000 rpm (0 to 60 s) to 7500 rpm (90 to 150 s). When increasing the LVAD speed from 7500 rpm (90 to 150 s) to 10,000 rpm (180 to 240 s), there was a larger S_{Hb+Mb} increase, from 20.7% to 38.4%. The S_{Hb+Mb} increased with LVAD pump speed ($p<0.001$, ANOVA). During the following phases with constant LVAD speed and variations in $F_{I,O2}$ 21%, (300 to 360 s), 50% (360 to 420 s), 100% (420 to 480 s), S_{Hb+Mb} increased significantly ($p<0.001$, ANOVA).

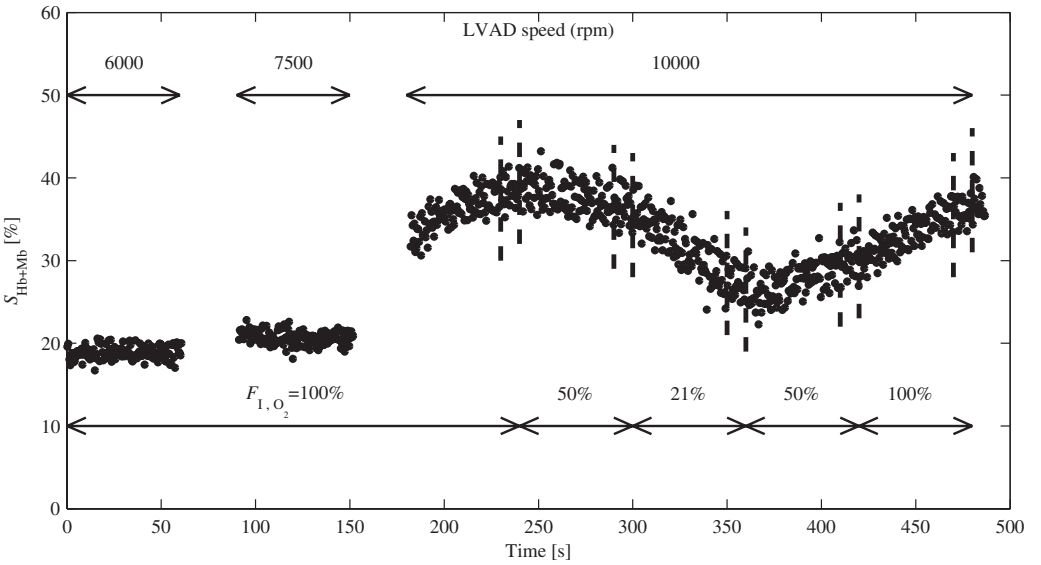

Fig. 6 S_{Hb+Mb} as a function of time during variations in LVAD speed and $F_{I,O2}$ in calf B1. Note: Last 10 s in each $F_{I,O2}$ phase are marked with vertical dashed lines.

4 Discussion

We have presented a calibrated diffuse reflectance spectroscopy method for *in vivo* determination of myocardial tissue light scattering properties and chromophore tissue fractions, as well as the sum of hemoglobin and myoglobin oxygenation and cytochrome oxidation. A custom-made fiber-optic probe was designed to enable intramyocardial probe placement. The method relies on an empirical light transport model together with calibration measurements on liquid optical phantoms,[21] which previously has been found applicable for *in vivo* determination of myocardial oxygenation.[22] The method was evaluated during hemodynamic and respiratory provocations in seven calves, enrolled in two different studies.

4.1 *Spectral Fitting*

In our previous study of myocardial oxygenation estimation with DRS,[22] we found characteristic spectral misfits in model adaption to measured spectra. For model I, the lowest R^2 value for the model adaption to measured spectra from group A, $F_{I,O2}$=21%, was 0.954. The corresponding value for the model II was R^2=0.994. Averaged over calves A1 to A5, the R^2 value improved from 0.965 (model I) to R^2=0.997 (model II). When using model II, the residual spectra, defined as $T^*_{cal,II}/M^{norm}_{heart}-1$, displayed no systematic trends as function of wavelength. Furthermore, the introduction of a fitting parameter in the model allowing wavelength shifting (up to ±5 nm)

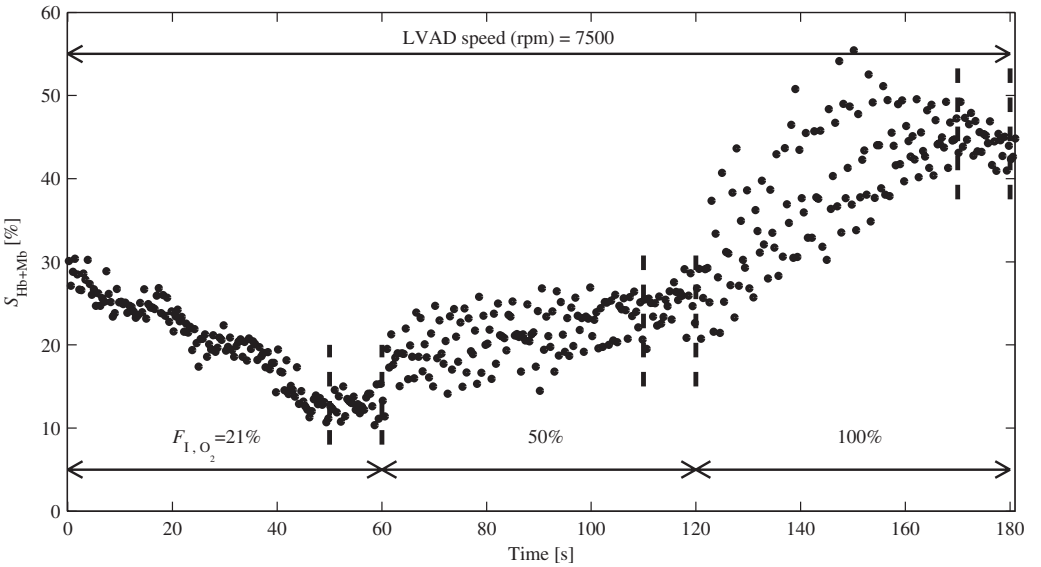

Fig. 7 S_{Hb+Mb} as a function of time during variations in $F_{I,O2}$ during constant LVAD speed (7500 rpm) in calf B2. Note: Last 10 s in each $F_{I,O2}$ phase are marked with vertical dashed lines.

Table 2 Average chromophore tissue fractions and S_{Hb+Mb} for the last 10 s of every phase.

Calf											
B1						B2					
LVAD speed	$F_{I,O2}$	f_{Hb+Mb}	S_{Hb+Mb}	f_{metHb}	$f_{cyt\ aa3}$	LVAD speed	$F_{I,O2}$	f_{Hb+Mb}	S_{Hb+Mb}	f_{metHb}	$f_{cyt\ aa3}$
[rmp]	[%]	[%]				[rmp]	[%]	[%]			
6000	100	0.8	18.8	0.2	1.8	7500	21	0.9	12.9	0[a]	2.1
7500	100	0.9	20.7	0.2	1.9	7500	50	0.9	25.1	0[a]	2.1
10,000	100	0.8	38.4	0.2	1.6	7500	100	0.9	44.3	0[a]	1.9
10,000	50	0.8	36.3	0.2	1.6						
10,000	21	0.8	27.1	0.2	1.6						
10,000	50	0.8	30.0	0.2	1.6						
10,000	100	0.8	36.5	0.2	1.6						

[a]Calculated values were smaller than 0.05%.

of hemoglobin absorption spectra, naturally contributed to the improved spectra fit compared to our previous study. When including additional chromophores, it is a necessity that their absorption spectra are unique for the chosen wavelength region. This means that none of the chromophores should have an absorption spectrum that could be expressed as a linear combination of other included chromophores. In this study, where the wavelength region 520 to 800 nm was used, all included chromophores displayed unique absorption spectra.

4.2 *Intramyocardial Light Scattering*

The estimated average value for μ_s' at 525 nm of 1.34 mm^{-1} in this study is comparable to that in pig hearts by Gandjbakhche et al.[32] ($\mu_s' = 1.2$ to 1.1 mm^{-1} at 540 to 590 nm)[32] Reported values by Häggblad et al. are in the range 0.42 to 1.3 mm^{-1} in wavelength region 530 nm to 585 nm.[22]

4.3 *Intramyocardial Tissue Chromophores*

4.3.1 *Hemo- and myoglobin*

The f_{Hb+Mb} values reported in Table 1 and Table 2 varied from 0.5% to 1.6% and displayed very small and nonsystematic intraindividual variations during changes in $F_{I,O2}$ and/or LVAD speed. The magnitude of f_{Hb+Mb} pulsations varied between cases, suggesting that large variations may indicate the presence of a large blood vessel, while smaller f_{Hb+Mb} variations may indicate a probe placement in an area dominated by capillaries. It should be noted that the magnitude of the variations in f_{Hb+Mb} may be affected by movement artifacts due to myocardial contractions, although it is fixated by epicardial suturing. Due to the contractile movement of the myocardium, it is likely that the pressure between the probe tip and the surrounding tissue varies. At such high pressure (contractile phase), Hb molecules in front of the probe may be forced away, causing f_{Hb+Mb} to drop.

When analyzing individual spectra, cyclic variations in f_{Hb+Mb} with identical frequency as the heart rate were observed. Since myoglobin is bound to muscle tissue,[33] it is reasonable to assume that variations in f_{Hb+Mb} should be associated with changes mostly in hemoglobin tissue fraction. Moreover, myoglobin is nearly fully oxygenated at normal working conditions,[18] and releases oxygen only at very low partial oxygen pressure,[34] which is not the case during the conditions in this study. Our observed variations in S_{Hb+Mb} should therefore be interpreted as a change mostly in hemoglobin oxygenation. The relationship between the pulsatile variations in the wavelength shift of the Hb spectrum and the S_{Hb+Mb} did not support the idea that the relative Hb and Mb contributions can be determined from the wavelength shift. However, the red-shift of Mb is small (about 5 nm), which demands very high wavelength accuracy in the recordings and also suggests that reference spectra obtained with the same spectrometer should be used.

We chose not to use more sophisticated methods for separation of hemoglobin and myoglobin oxygenation, despite the fact that other authors[14,35,36] have made successful attempts to distinguish between hemoglobin and myoglobin absorption influence on both *in vitro* and *in vivo* diffuse reflectance spectra recordings.

In the majority of cases, we observed a strong negative correlation between f_{Hb+Mb} and S_{Hb+Mb} If the assumptions of constant myoglobin tissue fraction and saturation (nearly 100%) holds true, a likely explanation for the negative S_{Hb+Mb} versus f_{Hb+Mb} correlation is that when f_{Hb+Mb} decreases, the relative influence of myoglobin absorption in the measured spectra increases, and since myoglobin is nearly fully oxygenated, S_{Hb+Mb} will increase. However, maximum S_{Hb+Mb} values of 33.3% (group A; A1) and 44.3% (group B; B2), respectively, suggest that the hemoglobin absorption contribution is predominant throughout the measurements.

In group A, 4 of 5 calves responded with increased S_{Hb+Mb} values when inspired $F_{I,O2}$ was increased. During ventilation with room air ($F_{I,O2}$=21%), the average S_{Hb+Mb} was 20.0%, which corresponds to an myocardial oxygen uptake of 80%, which is in agreement with findings from several other studies.[37–39]

In calf B1, a small increase in S_{Hb+Mb} was found when increasing LVAD speed from 6000 rpm to 7500 rpm. When the LVAD speed was further increased to 10,000 rpm, S_{Hb+Mb} drastically increased. During all three LVAD speed settings, the $F_{I,O2}$ was held at 100%. For the following changes in $F_{I,O2}$ levels during constant LVAD speed, the S_{Hb+Mb} displayed the same trend as in calves A1 to A4.

When increasing $F_{I,O2}$ in calf B2, S_{Hb+Mb} increased from 12.9% ($F_{I,O2}$=21%) to 44.3% ($F_{I,O2}$=100%).

The finding that S_{Hb+Mb} increased with LVAD pump speed was expected, since the purpose of the LVAD is to lower the amount of work needed (and hence lower the oxygen consumption) in the left ventricle, to maintain sufficient systemic and coronary circulation.

4.3.2 *Cyt aa3 and metHb*

The $f_{cyt\ aa3}$ values reported in Table 1 and Table 2 varied from 1.2% to 2.0% and displayed very small and nonsystematic intraindividual variations during changes in $F_{I,O2}$ and/or LVAD speed. By assuming a molecular weight of 200 kDa for cyt aa3 (Ref. 40), the findings for $f_{cyt\ aa3}$ gives a cyt aa3 tissue concentration ranging from 60 to 100 nmol·g^{-1} tissue wet weight. Reported values for porcine heart *in vitro* are 30.5 nmol·g^{-1} tissue wet weight.[41]

The findings of $O_{cyt\ aa3}$ above 96% in both group A and group B, despite low S_{Hb+Mb} are compatible with findings in pig hearts during LAD occlusion.[17] In Parson's study, $O_{cyt\ aa3}$ decreased only when LAD flow was reduced by more than 40% of resting flow.[17] The nonrestricted coronary flow and normoxic conditions present throughout the measurements did not, as expected, display any reduction of the $O_{cyt\ aa3}$.

The obtained fractions of methemoglobin were in the interval 0 to 0.2%, which is in agreement with values reported by Wright et al.[42]

5 Conclusions

By using a calibrated intramuscular probe, the tissue chromophore fractions and the hemoglobin+myoglobin oxygenation and cyt aa3 oxidation status of the myocardial chromophores during respiratory and hemodynamic provocations can be monitored. The presented DRS analysis algorithm is capable of delivering results that are physiologically reasonable and in agreement with others. Model inclusion of the chromophores metHb, cyt aa3, ox, and cyt aa3, red, in addition to Hb, HbO_2, and W, resulted in nonsystematic residual spectra.

The presented diagnostic tool follows the way of the oxygen from hemo- and myoglobin to the last step of the oxidative phosphorylation and has the potential for enabling early detection of tissue hypoxia in the heart. However, future studies should include coronary flow provocations and pharmaceutically induced alterations of the mitochondrial ability to utilize oxygen in the ATP formation process. Furthermore, in these future studies, it would be advisable to include, in addition to the presented DRS technique, additional measurement techniques such as microdialysis for cellular metabolism analysis[43] and intermittent coronary sinus blood samples for global *in vitro* analysis of hemoglobin oxygenation.

Appendix

The absorption data for all chromophores are given in specific extinction coefficients (μ_e) [mM^{-1}·cm^{-1}]. To be included in the light transport model, μ_e has to be translated into the absorption coefficient μ_a [mm^{-1}]. A general description of this conversion has been described by Prahl[44] and is shown in Eq. (5);

$$\mu_a = 100 \cdot \frac{\ln(10) \cdot \mu_e \cdot \rho}{m_w}, \tag{5}$$

where ρ is the substance density [g·L^{-1}], and m_w is the molecular weight [g·mol^{-1}] of the specific substance.

For the hemoglobin protein, consisting of four heme units, the molecular weight was set to 64,500 $g \cdot mol^{-1}$. For cyt aa3, where each functional unit consists of 13 subunit enzymes containing haem a, haem a3, CuA, and CuB, the molecular weight was set to 200,000 $g \cdot mol^{-1}$. To convert the specified tissue fractions to a molecular amount (e.g., mol per gram tissue), simply divide the fraction by the corresponding molecular weight.

Acknowledgments

This study was financed by VINNOVA and Perimed AB through the SAMBIO research collaboration program between companies and academia within bioscience (VINNOVA, D. no. 2008-00149), by the Swedish Research Council (D. no. 2005-3934), and by NovaMedTech (supported by the European union Regional Development Fund). The authors would also like to thank the staff at the Laboratory for Experimental Animal Studies, Faculty of Health Sciences, Linköping University.

References

1. R. I. Williams, R. Haaverstad, G. Sianos, E. Vourvouri, and A. G. Fraser, "Perioperative tissue Doppler echocardiography and bypass graft flowmetry in patients undergoing coronary revascularization: predictive power for late recovery of regional myocardial function," *J. Am. Soc. Echocardiogr* **15**(10, II), 1202–1210 (2002).
2. R. Haaverstad, N. Vitale, O. Tjomsland, A. Tromsdal, H. Torp, and S. O. Samstad, "Intraoperative color Doppler ultrasound assessment of LIMA-to-LAD anastomoses in off-pump coronary artery bypass grafting," *Ann. Thorac. Surg.* **74**(4), 1390–1394 (2002).
3. L. Lovstakken, K. S. Ibrahim, N. Vitale, S. T. Henriksen, I. Kirkeby-Garstad, H. Torp, and R. Haaverstad, "Blood flow imaging: a new two-dimensional ultrasound modality for enhanced intraoperative visualization of blood flow patterns in coronary anastomoses," *J. Am. Soc. Echocardiogr* **21**(8), 969–975 (2008).
4. W. J. Parsons, J. C. Rembert, R. P. Bauman, J. C. Greenfield Jr., and C. A. Piantadosi, "Dynamic mechanisms of cardiac oxygenation during brief ischemia and reperfusion," *Am. J. Physiol. Heart Circ. Physiol.* **259**(5), 1477–1485 (1990).
5. M. K. Al-Obaidi, P. J. Etherington, D. J. Barron, C. P. Winlove, and J. R. Pepper, "Myocardial tissue oxygen supply and utilization during coronary artery bypass surgery: evidence of microvascular no-reflow," *Clin. Sci.* **98**(3), 321–328 (2000).
6. Y. Chung, "Oxygen reperfusion is limited in the postischemic hypertrophic myocardium," *Am. J. Physiol. Heart Circ. Physiol.* **290**(5), H2075–H2084 (2006).
7. F. W. Heineman, V. V. Kupriyanov, R. Marshall, T. A. Fralix, and R.

S. Balaban, "Myocardial oxygenation in the isolated working rabbit heart as a function of work," *Am. J. Physiol. Heart Circ. Physiol.* **262**(1), 255–267 (1992).
8. J. R. Leisey, D. A. Scott, L. W. Grotyohann, and R. C. Scaduto Jr., "Quantitation of myoglobin saturation in the perfused heart using myoglobin as an optical inner filter," *Am. J. Physiol. Heart Circ. Physiol.* **267**(2), 645–653 (1994).
9. J. R. Zijp and J. J. Ten Bosch, "Optical properties of bovine muscle tissue *in vitro*: a comparison of methods," *Phys. Med. Biol.* **43**(10), 3065–3081 (1998).
10. K. A. Schenkman, "Cytochrome c oxidation determined by multi-wavelength optical spectral analysis in the isolated perfused heart," *Proc. SPIE* **4613**, 278–285 (2002).
11. C. Ribacka, "Redox-linked proton transfer by cytochrome c oxidase," PhD Thesis, Department of Biological and Environmental Sciences, University of Helsinki (2007), p. 64.
12. L. H. Opie, *Heart Physiology from Cell to Circulation*, 4th ed., Lippincott, Williams & Wilkins, Philadelphia, PA (2004).
13. C. E. Cooper and R. Springett, "Measurement of cytochrome oxidase and mitochondrial energetics by near-infrared spectroscopy," *Philos. Trans. R. Soc. London, Ser. B* **352**(1354), 669–676 (1997).
14. K. A. Schenkman, D. R. Marble, E. O. Feigl, and D. H. Burns, "Near-infrared spectroscopic measurement of myoglobin oxygen saturation in the presence of hemoglobin using partial least-squares analysis," *Appl. Spectrosc.* **53**(3), 325–331 (1999).
15. A. Mayevsky and B. Chance, "Oxidation-reduction states of NADH *in vivo*: from animals to clinical use," *Mitochondrion* **7**(5), 330–339 (2007).
16. F. F. Jöbsis, J. H. Keizer, J. C. LaManna, and M. Rosenthal, "Reflectance spectrophotometry of cytochrome aa3 *in vivo*," *J. Appl. Physiol.: Respir., Environ. Exercise Physiol.* **43**(5), 858–872 (1977).
17. W. J. Parsons, J. C. Rembert, R. P. Bauman, F. G. Duhaylongsod, J. C. Greenfield Jr., and C. A. Piantadosi, "Myocardial oxygenation in dogs during partial and complete coronary artery occlusion," *Circ. Res.* **73**(3), 458–464 (1993).
18. A. E. Arai, C. E. Kasserra, P. R. Territo, A. H. Gandjbakhche, and R. S. Balaban, "Myocardial oxygenation *in vivo*: optical spectroscopy of cytoplasmic myoglobin and mitochondrial cytochromes," *Am. J. Physiol. Heart Circ. Physiol.* **277**(2), 683–697 (1999).
19. "BORL Tissue Spectra," available at http:www.medphys.ucl.ac.uk/research/borl/research/NIR_topics/spectra/spectra.htm (retrieved 10 June 2009).
20. L. Hübbert, B. Peterzén, S. Träff, B. Janerot-Sjöberg, and H. Ahn, "Axial flow pump treatment during myocardial depression in calves: an invasive hemodynamic and echocardiographic tissue Doppler study," *ASAIO J.* **54**, 367–371 (2008).
21. S. L. Jacques, "Optical fiber reflectance spectroscopy," available at http://omlc.ogi.edu/news/oct03/saratov/index.htm (retrieved 10 June 2009).
22. E. Häggblad, T. Lindbergh, M. G. D. Karlsson, H. Casimir-Ahn, E. G. Salerud, and T. Strömberg, "Myocardial tissue oxygenation estimated with calibrated diffuse reflectance spectroscopy during coronary artery bypass grafting," *J. Biomed. Opt.* **13**(5), 054030 (2008).
23. P. R. Bargo, S. A. Prahl, T. T. Goodell, R. A. Sleven, G. Koval, G. Blair, and S. L. Jacques, "*In vivo* determination of optical properties of normal and tumor tissue with white light reflectance and an empirical light transport model during endoscopy," *J. Biomed. Opt.* **10**(3), 034018 (2005).
24. T. Lindbergh, I. Fredriksson, M. Larsson, and T. Strömberg, "Spectral determination of a two-parametric phase function for polydispersive scattering media," *Opt. Express* **17**(3), 1610–1621 (2009).
25. J. Lee, N. El-Abaddi, A. Duke, A. E. Cerussi, M. Brenner, and B. J. Tromberg, "Noninvasive *in vivo* monitoring of methemoglobin formation and reduction with broadband diffuse optical spectroscopy," *J. Appl. Phys.* **100**(2), 615–622 (2006).
26. S. Fleischer, G. Rouser, B. Fleischer, A. Casu, and G. Kritchevsky, "Lipid composition of mitochondria from bovine heart, liver, and kidney," *J. Lipid Res.* **8**(3), 170–180 (1967).
27. D. Y. Fei and K. K. Shung, "Ultrasonic backscatter from bovine tissues," in *IEEE Ultrasonics Symposium*, pp. 677–680, IEEE, Piscataway, NJ (1984).
28. B. A. Wittenberg, J. B. Wittenberg, and I. R. Katz, "Oxygen transport in isolated cardiac myocytes," *Basic Res. Cardiol.* **80**, 75–77 (1985).
29. J. Nocedal and S. J. Wright, "Algorithms for nonlinear least-squares problems," Chapter 10.3, in *Numerical Optimization*, T. V. Mikosh, S. M. Robinson, and S. I. Resnick, Eds., pp. 258–262, Springer Science and Business Media, New York (2008).
30. W. G. Zijlstra, A. Buursma, and O. W. van Assendelft, "Definitions and terminology," Chapter 2, in *Visible and Near Infrared Absorption Spectra of Human and Animal Haemoglobin–Determination and Application*, pp. 9–16, VSP, Ridderkerk, The Netherlands (2000).
31. H. Buiteveld, J. M. H. Hakvoort, and M. Donze, "The optical properties of pure water," in *Ocean Optics XII*, J. S. Jaffe, Ed., *Proc. SPIE* **2258**, 174–183 (1994).
32. A. H. Gandjbakhche, R. F. Bonner, A. E. Arai, and R. S. Balaban, "Visible-light photon migration through myocardium *in vivo*," *Am. J. Physiol. Heart Circ. Physiol.* **277**(2), 698–704 (1999).
33. G. J. Tortora and S. Reynolds Grabowski, "The cardiovascular system: Blood vessels and hemodynamics," Chapter 21, in *Principles of Anatomy and Physiology*, B. Roesch, Ed., pp. 696–756, John Wiley & Sons, Inc., Hoboken, NJ (2003).
34. K. A. Schenkman, D. R. Marble, D. H. Burns, and E. O. Feigl, "Myoglobin oxygen dissociation by multiwavelength spectroscopy," *J. Appl. Physiol.* **82**(1), 86–92 (1997).
35. K. A. Schenkman, D. R. Marble, D. H. Burns, and E. O. Feigl, "Optical spectroscopic method for *in vivo* measurement of cardiac myoglobin oxygen saturation," *Appl. Spectrosc.* **53**(3), 332–338 (1999).
36. L. S. L. Arakaki, M. J. Kushmerick, and D. H. Burns, "Myoglobin oxygen saturation measured independently of hemoglobin in scattering media by optical reflectance spectroscopy," *Appl. Spectrosc.* **50**(6), 697–707 (1996).
37. B. I. Levy, E. Pinard, and J.-B. Michel, "Transmural gradient of tissue gas tensions in the canine left ventricular myocardium during coronary clamping and reactive hyperemia," *Pflugers Archiv. Eur. J. Physiol.* **407**(4), 388–395 (1986).
38. J. Vinten-Johansen and H. R. Weiss, "Oxygen consumption in subepicardial and subendocardial regions of the canine left ventricle. The effect of experimental acute valvular aortic stenosis," *Circ. Res.* **46**(1), 139–145 (1980).
39. T. M. Nosek, *Essentials of Human Physiology*, Medical College of Georgia, http://imc.meded.com/integrated/demos/hpdemo/program/start.htm (Last retrieval date 8 Apr. 2010).
40. S. Ferguson-Miller, "Mammalian cytochrome c oxidase, a molecular monster subdued," *Science* **272**(5265), 1125 (1996).
41. R. S. Balaban, V. K. Mootha, and A. Arai, "Spectroscopic determination of cytochrome c oxidase content in tissues containing myoglobin or hemoglobin," *Anal. Biochem.* **237**(2), 274–278 (1996).
42. R. O. Wright, W. J. Lewander, and A. D. Woolf, "Methemoglobinemia: etiology, pharmacology, and clinical management," *Ann. Emerg. Med.* **34**(5), 646–656 (1999).
43. J. Pöling, A. Leptien, S. Klaus, W. Rees, E. Kraatz, K. Wiebe, and L. Bahlmann, "Analysis of the myocardial metabolism by microdialysis during open beating heart surgery," *Scand. Cardiovasc. J.* **41**(2), 114–119 (2007).
44. S. A. Prahl, "Optical absorption of hemoglobin," available at http://omlc.ogi.edu/spectra/hemoglobin/index.html (retrieved 10 June 2009).